

ARTICLE OPEN



Three-dimensional imaging of ferroaxial domains using circularly polarized second harmonic generation microscopy

Hiroyuki Yokota^{1,2✉}, Takeshi Hayashida³, Dan Kitahara¹ and Tsuyoshi Kimura³

The spontaneous symmetry breakdown of matter is one of the most important concepts in materials physics and leads to a phase transition into an ordered phase and domain formation in its consequence. The so-called ‘ferroaxial order’ characterized by a rotational structural distortion with an axial vector symmetry has gained growing interest as a new class of ordered state. However, the observation of ferroaxial domain states, that is, clockwise and counterclockwise rotational states, is not straightforward and has been little investigated. Here, we propose that the circular intensity difference in second harmonic generation (CID-SHG) offers an experimental technique to investigate ferroaxial order and its domain states through the transition process of higher-order multipoles such as magnetic-dipole and electric-quadrupole. By using CID-SHG microscopy, we successfully visualize three-dimensional images of ferroaxial domain structures in NiTiO₃. Our results indicate that CID-SHG is a sensitive probe of ferroaxial order and opens possibilities for the use of ferroaxial materials in nonlinear optical manipulations.

npj Quantum Materials (2022)7:106; <https://doi.org/10.1038/s41535-022-00515-w>

INTRODUCTION

Ferroics are defined as materials possessing some sort of switchable ordering that comes about spontaneously^{1,2}. The ferroaxial order, which is characterized by a rotational structural distortion in a crystal, has been proposed as a new class of ferroic order in recent years^{3–5}. Such a rotational distortion is regarded as a vortex of electric dipole moments, an example of which is illustrated in Fig. 1a. The order parameter of the ferroaxial order is the so-called ferroaxial moment **A** (or sometimes called electric toroidal moment) defined as $\mathbf{A} \propto \sum_i \mathbf{r}_i \times \mathbf{p}_i$ where \mathbf{r}_i is a position vector of an electric dipole \mathbf{p}_i at i site from a symmetrical center of the rotation^{6–8}. Though **A** is symmetric under both time reversal and space inversion, it breaks the mirror symmetry whose mirror plane includes the rotation axis. Thus, ferroaxial order results in the formation of two domain states with the opposite signs of **A** (Fig. 1a, b). Note that a mirror symmetry with the mirror plane perpendicular to the rotation axis is not necessarily broken in ferroaxial order, which is distinct from chirality.

Until recently, ways to identify the sign of **A** or ferroaxial domain states have not been common as those of chirality with the use of symmetry-dependent physical phenomena, such as optical activity. In these few years, however, domain states of ferroaxial order were experimentally demonstrated by using rotational anisotropy second harmonic generation (SHG)^{9,10} and electrogyration (EG)^{11,12}. Motivated by the experimental progress, ferroaxial order has attracted growing interest because of its potential for unconventional physical phenomena and new functionalities. For example, it is expected that ferroaxial order causes transverse responses in which input external fields (magnetic field, electric field, and current) induce output conjugate physical quantities (magnetic, electric, and toroidal dipoles, respectively) along the direction perpendicular to both **A** and the applied field^{13,14}. As another example, it is theoretically proposed that the application of thermal gradient to ferroaxial insulator induces electric polarization perpendicular to the thermal gradient¹⁵.

In this study, we propose an experimental method for three-dimensional imaging of ferroaxial domains, which is based on the circular intensity difference in the optical SHG signal (CID-SHG) from a ferroaxial crystal. SHG is a phenomenon in which coherent light with a frequency twice of a fundamental wave is generated through the second-order nonlinear interaction between light and material¹⁶. Due to its sensitivity to symmetry breaking of either spatial or time-reversal operation, it has been widely used to observe the phase transition and visualize the domain structure in ferroics¹⁷. Typically, the electric-dipole (ED) contribution is dominant in SHG, and the ED-induced SHG is strictly forbidden in systems with inversion symmetry. Therefore, SHG is usually applied to non-centrosymmetric materials or the surface or interface where the discontinuity breaks the inversion symmetry. Furthermore, SHG using circularly polarized light offers a highly sensitive probe of molecular systems, biomaterials, and surfaces with chiral structures^{18–20}. In centrosymmetric systems, however, SHG is allowed if higher-order multipole contributions such as magnetic-dipole (MD) or electric-quadrupole (EQ) contributions are involved. Additionally, the enhancement of SHG has been reported near an optical resonance and is used to observe the domain structure in the case of $d-d$ transition in magnetics^{17,21}. Previous studies on the investigation of ferroaxial order in some ferroaxial materials utilized rotational anisotropy SHG which is ascribed to the EQ contribution^{9,10}.

Here we adopt CID-SHG to identify the sign of ferroaxial moment and to visualize ferroaxial domains in an order-disorder type ferroaxial crystal, NiTiO₃, belonging to a centrosymmetric structure with the space group of $R\bar{3}$ (Supplementary Note 1). The idea is inspired by a report on the observation of SHG dependent on circular polarization of fundamental light in the paramagnetic phase of another ilmenite-type compound, MnTiO₃²². The CID-SHG of MnTiO₃ is interpreted in the framework of the MD contribution. We apply this effect to examine ferroaxial order in NiTiO₃ and achieve three-dimensional imaging of its ferroaxial

¹Department of Physics, Chiba University, 1-33 Yayoi-cho, Inage-ku, Chiba-shi, Chiba 263-8522, Japan. ²JST PRESTO, 7 Goban-cho, Chiyoda-Ku, Tokyo 102-0076, Japan.

³Department of Advanced Materials Science, University of Tokyo, Kashiwa, Chiba 277-8561, Japan. ✉email: hiroyuki.yokota@chiba-u.jp

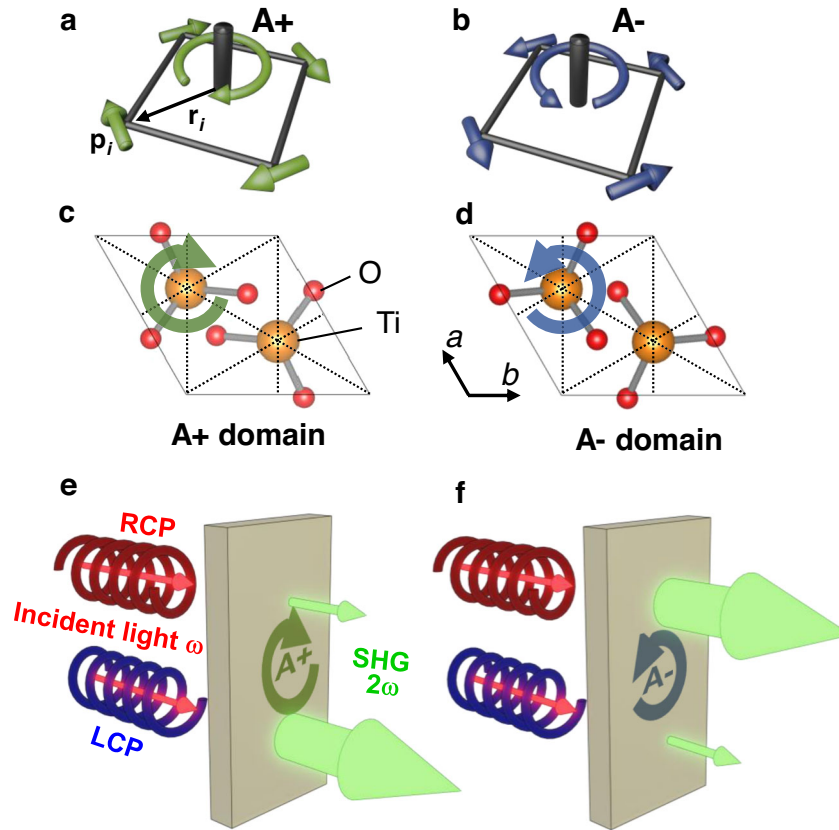


Fig. 1 Circular intensity difference (CID) in second harmonic generation (SHG) from ferroaxial materials. **a, b** Schematic illustrations of a pair of ferroaxial domain states with the opposite sign of ferroaxial moment \mathbf{A} defined as $\mathbf{A} \propto \sum_i \mathbf{r}_i \times \mathbf{p}_i$. Here \mathbf{r}_i denotes a position vector of electric dipole \mathbf{p}_i from the symmetrical center of a structural unit. **c, d** Simplified c -axis views of a pair of ferroaxial domain states (A+ and A- domains) in NiTiO₃. **e, f** Conceptual diagram of CID-SHG from A+ and A- domain states. The red and light green arrows denote fundamental circularly polarized light and SHG, respectively. The size of the light green arrows represents the intensity of SHG. Thus, the intensity of SHG from a ferroaxial material depends on both the circular polarization of fundamental light and the sign of \mathbf{A} .

domain structures from the surface into the material depth with a sub-micrometer resolution.

RESULTS AND DISCUSSION

Formulation of circular intensity difference in second harmonic generation

At room temperature, the crystal structure of NiTiO₃ is the ilmenite-type with the ferroaxial point group $\bar{3}$ in which Ni and Ti layers are stacked alternately along the hexagonal c axis²³. Depending on the ordered sequence (Ni-Ti-Ni-Ti or Ti-Ni-Ti-Ni), two ferroaxial domain states (A+ and A- domains) are formed¹¹, as schematically illustrated in Fig. 1c, d. In the following, we derive CID-SHG of the system with the ferroaxial point group $\bar{3}$. Though this point group is centrosymmetric and forbids the ED-induced SHG, it allows the MD- and EQ-induced SHG. MD and EQ contributions can be represented by the axial tensor of rank 3 and the polar tensor of rank 4, respectively. The equations for SHG in the point group $\bar{3}$ for MD and EQ contributions have been derived in ref. ²². These two contributions provide the same expressions of SHG and calculating both contributions gives us more terms without any quantitative differences (Supplementary Note 2). Therefore, for simplicity, we omit the EQ contribution and take only the MD contribution in the following discussion.

We set the orthogonal axes xyz with z along the light propagation direction. The nonlinear magnetization \mathbf{M} induced by MD is described by

$$M_i^{\text{MD}}(2\omega) \propto \chi_{ijk}^{\text{MD}} E_j(\omega) E_k(\omega), \quad (1)$$

where χ_{ijk}^{MD} is the third-rank nonlinear optical susceptibility tensor and E is an electric field. In the wave equation for the electric field, the MD contribution leads to a source term $\mu_0 \nabla \times \partial \mathbf{M}^{\text{MD}} / \partial t$ for SHG. When the light propagation direction ($\parallel z$) is parallel to the c axis (hexagonal setting), there are only two independent components to be considered $\chi^{(1)} = \chi_{xxx} = -\chi_{xyy} = -\chi_{yyx} = -\chi_{yxx}$ and $\chi^{(2)} = \chi_{yyy} = -\chi_{xxy} = -\chi_{xyx} = -\chi_{yxx}$ ²⁴. The total source term obtained under the present geometry can be described as

$$\mathbf{S} \propto \left\{ \chi^{(2)} (E_x^2 - E_y^2) + 2\chi^{(1)} E_x E_y \right\} \mathbf{e}_x + \left\{ \chi^{(1)} (E_x^2 - E_y^2) - 2\chi^{(2)} E_x E_y \right\} \mathbf{e}_y, \quad (2)$$

where $\mathbf{e}_{x(y)}$ denotes the unit vector along $x(y)$. When the fundamental light is close to the absorption edge, we need to consider the resonance SHG having the complex susceptibility tensors ($\chi = \chi' + i\chi''$). In this case, the second harmonic (SH) intensity obtained under circularly polarized light can be calculated as follows:

$$I \propto \left(|\chi^{(1)}|^2 + |\chi^{(2)}|^2 \right) (E_+^4 + E_-^4) + 2 \left(\chi^{(2)'} \chi^{(1)'} - \chi^{(2)''} \chi^{(1)''} \right) (E_+^4 - E_-^4), \quad (3)$$

where E_{\pm} represents the two components of circular polarization. The second term of Eq. (3) depends on the circular polarization of the fundamental light. This means that the SH intensity obtained by right-handed circularly polarized (RCP) fundamental light differs from that by left-handed circularly polarized (LCP) one in the system with the point group $\bar{3}$.

Furthermore, let us consider the effect of ferroaxial domains on the SH intensity I . A+ and A- domains are converted with each

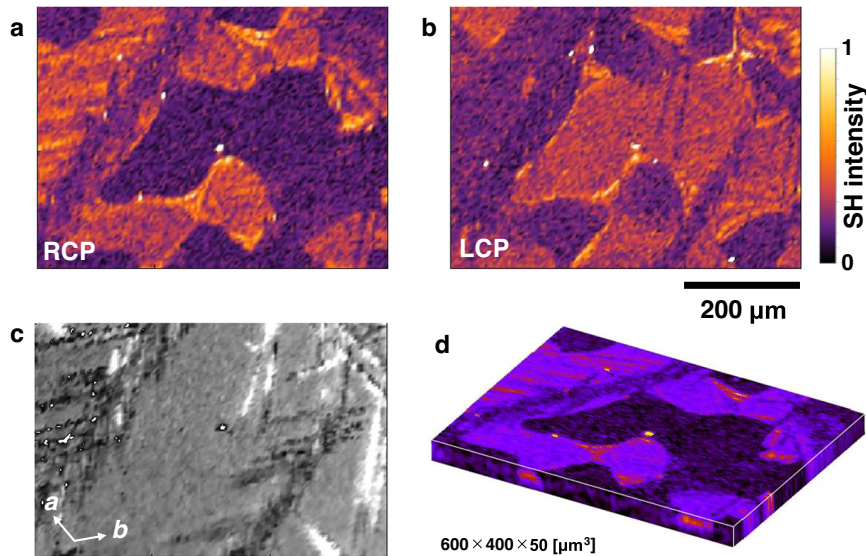


Fig. 2 SHG imaging of ferroaxial domains in NiTiO₃ using circularly polarized fundamental light. **a, b** Two-dimensional maps of SH intensity obtained with (a) right-handed circularly polarized (RCP) and (b) left-handed circularly polarized (LCP) light. Bright and dark regions correspond to either A+ or A− ferroaxial domains. **c** Transmission optical microscopy image of the area corresponding to the SHG images of (a) and (b). Branch-like patterns in (c) correspond to TiO₂ impurities. **d** Three-dimensional image of SH intensity at the same area as (a) and (b).

other by the mirror operation with the mirror plane parallel to (110). This mirror operation leads to the sign change of $\chi^{(2)}$ but not $\chi^{(1)}$ (Supplementary Note 3). Therefore, the sign of the second term of Eq. (3) in the A+ domain is opposite to that of the A− domain. Thus, we can identify the ferroaxial domain state through CID-SHG. Furthermore, spatially resolved measurements such as SHG microscopy using circularly polarized fundamental light allow the visualization of ferroaxial domain structures. The conceptual diagrams of CID-SHG from ferroaxial domains are illustrated in Fig. 1e, f. Under RCP fundamental light, one domain (A+ domain state) exhibits weaker SHG while the other one (A− domain state) exhibits stronger SHG. The situation becomes the opposite when LCP fundamental light is irradiated.

Visualization of ferroaxial domains

We apply the discussion above, namely, CID-SHG between A+ and A− domains, to the visualization of ferroaxial domain structures in NiTiO₃. We measured spatial distributions of SH intensity in single crystals of NiTiO₃ by SHG microscopy using circularly polarized fundamental light irradiated along the *c* axis (see “Methods” and ref. 25). For this measurement, we prepared samples with multi-domain states by a proper annealing procedure (see “Methods” and ref. 12). Figure 2c shows the optical transmission microscope image of the (001) face of a sample. In the image, branch-like patterns are seen and correspond to TiO₂ impurities. Except for these impurities, the sample is homogeneous, and it is impossible to distinguish ferroaxial domain states in the microscope image. Figure 2a, b shows the two-dimensional SHG images obtained with RCP and LCP fundamental light with a wavelength of 1200 nm, respectively. These images were collected from the same area as that in Fig. 2c. Bright and dark correspond to high- and low-intensity counts, respectively. The magnitude of the normalized CID-SHG in each area, defined as $|\Delta I/I_{AVE}|$ where $\Delta I = (I_{RCP} - I_{LCP})$ and $I_{AVE} = (I_{RCP} + I_{LCP})/2$, is 0.6–1.3, meaning that SHG signals from NiTiO₃ strongly depend on circular polarization of incident light. In Supplementary Fig. 2, we show $\Delta I/I_{AVE}$ as a function of wavelength of fundamental light in an area where I_{RCP} is larger than I_{LCP} . $\Delta I/I_{AVE}$ gradually decreases with increasing the wavelength from 1200 to 1380 nm. This wavelength range corresponds to the Ni²⁺ *d*–*d* transition from the ³A_{2g} ground state to the ³T_{2g} state^{26,27}. The color contrast is reversed from the

image of Fig. 2a to Fig. 2b except in the impurity regions. Considering the discussion above, the bright and the dark regions correspond to a pair of ferroaxial domains with the opposite sign of ferroaxial moment. The observed domains are irregular in shape with size on a submillimeter scale.

To further confirm that spatial distributions of the color contrast in Fig. 2a, b reflect ferroaxial domain structures, we compared a CID-SHG image and a ferroaxial domain pattern obtained by an EG measurement^{11,12} (see also Supplementary Note 4). Supplementary Fig. 3a, b show CID-SHG images of another sample by using RCP and LCP fundamental light, respectively. The contrast reversal is also observed in this sample. Comparing the CID-SHG images (Supplementary Fig. 3a, b) with that obtained by the EG measurement (Supplementary Fig. 3c), their domain patterns well match up with each other. This supports that the area with bright and dark colors in CID-SHG images corresponds to different ferroaxial domain (A+ and A−) states. Thus, we confirm that CID-SHG is effective to visualize ferroaxial domain structures. Compared with other experimental techniques such as measurements of rotational anisotropy SHG and EG, the present CID-SHG measurement has the benefit of a large difference in its signals between A+ and A− domains, $[I_{RCP}(A+) - I_{RCP}(A-)] / \{ [I_{RCP}(A+) + I_{RCP}(A-)] / 2 \} = 32\%$. This is large enough to easily distinguish A+ and A− domains. In addition, another merit of CID-SHG is the availability to construct three-dimensional images without any destruction of the specimen. Figure 2d shows a three-dimensional image of SH wave distribution under an RCP fundamental light. The magnitude of SH intensity is nearly constant as a function of sample depth, which means the SH activity remains inside the sample and is not ascribed to the surface effect.

Next, to clarify SHG signals around a domain boundary (DB), we closely looked at the area near the DB. Figure 3a–c display magnified views of two-dimensional SHG images obtained with different polarization of fundamental light in the same area. On the right side of each panel, a cross-sectional profile along a white dashed line is attached. In the images with RCP and LCP fundamental light (Fig. 3a, b), in addition to CID-SHG between A+ and A− domains, a remarkable enhancement of SH intensity at DB is evident. Such an enhancement of SHG at DB is also seen for a measurement using linearly polarized fundamental light, which is displayed in Fig. 3c. The SH intensity is weak in both

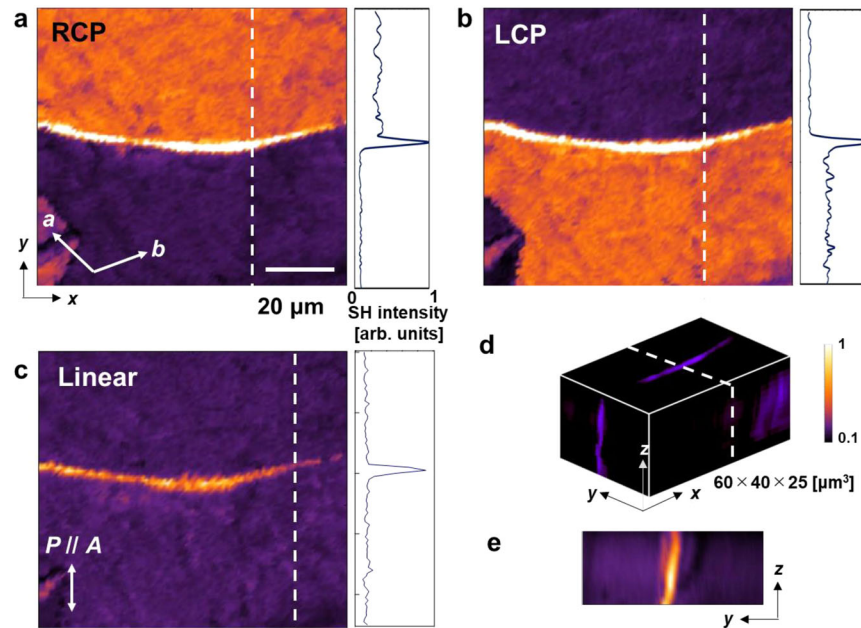


Fig. 3 Polarization dependence of circular intensity difference in second harmonic generation (SHG) around a ferroaxial domain boundary. **a, b** Two-dimensional maps of SH intensity obtained with (a) RCP, (b) LCP, and (c) linearly polarized fundamental light. Right panels of (a–c) show the profiles of SH intensity along the white dashed lines of the respective images. In (a), the crystallographic axes are indicated as white arrows. The white arrow embedded in (c) corresponds to the polarization directions of fundamental light and SHG. The upper and the lower areas with different SH intensities by measurements using circularly polarized light correspond to either A+ or A− ferroaxial domains. Regardless of the light polarization, the SH intensity is enhanced at the domain boundary. **d** Three-dimensional image of SH intensity at the same area as (a–c). **e** Depth profile in a plane cut at the white dashed line in (d). The bright line represents the depth profile of the domain boundary.

upper and lower domains, but the SH intensity at DB is around 3–10 times stronger than those from domains. Thus, the enhancement of SHG at DB is observed regardless of the polarization state of fundamental light. We also measured a depth profile of SH intensity using linearly polarized light in the area corresponding to Fig. 3c. Figure 3d shows a three-dimensional image of SH intensity, and its cross sectional cut at the position of the white dashed line is displayed in Fig. 3e. This result shows that the DB is almost perpendicular to the sample surface with keeping almost the same SH intensity. Thus, the enhancement of SH intensity at DB is not the surface effect but the bulk effect.

Although the materials themselves possess centro-symmetry and are non-polar, the emergence of polar nature at DBs has been observed in various ferroelastic materials such as CaTiO_3 ^{28,29} and LaAlO_3 ³⁰. In these materials, flexoelectric effect would play a major role to induce the polarization at DBs. Compared with the results of ferroelastics, the signal to noise ratio of SH intensity from ferroaxial DBs in NiTiO_3 is rather weak. It is not surprising since ferroaxial domain itself also produces SH intensity through MD or EQ contribution which is not the case for ferroelastic materials. If ferroaxial DB also possessed finite electric polarization which contributes to the ED-induced SHG, we could observe the drastic intensity difference between domain and DB since the ED contribution is typically much larger than other ones. Therefore, we do not claim that DBs of NiTiO_3 is polar. As a possible explanation of the enhancement of SHG at DBs, nonlinear Čerenkov SHG can be considered. Čerenkov SHG normally appears in a planner waveguide, and is recently used to visualize ferroelastic domain boundaries^{31,32}. Furthermore, at some DBs, characteristic fringe-like patterns are observed (see Supplementary Fig. 3d). By comparing the SHG image (Supplementary Fig. 3d) and the EG image (Supplementary Fig. 3c), we find that the fringe-like patterns in the SHG image often appear at green colored areas in the EG image. The green colored areas in the EG

image are considered to correspond to thick DBs which are not parallel to the *c* axis but considerably tilted from the *c* axis¹¹. Furthermore, a period of the fringe monotonically increases with increasing the wavelength of incident light (not shown). These results suggest that the interference of SHG produced in neighboring ferroaxial domains with tilted angles also contributes to SHG signals at DBs. However, more detailed experiments and analyses will be required to confirm the origin of the enhancement of SHG at DBs.

In summary, we investigated ferroaxial order in an order-disorder type ferroaxial material, NiTiO_3 , by SHG microscopy using circularly polarized fundamental light. Remarkable CID-SHG with the relative difference of SH intensity more than 60 % was observed between ferroaxial domains with the opposite sign of the ferroaxial moment. The results are well explained qualitatively by considering the transition process of higher-order multipoles such as magnetic-dipole and electric-quadrupole. With the large value of CID-SHG, we succeeded in the three-dimensional visualization of ferroaxial domains. Furthermore, we confirmed that spatial distributions of CID-SHG are nothing other than ferroaxial domains in comparison with the results of EG in the same sample. Compared with other techniques such as rotational anisotropy SHG and EG measurements, the CID-SHG method has the advantage in terms of three-dimensional spatial resolution and electrode-free method, and so on. Thus, the application of CID-SHG beyond the ED approach offers a powerful technique for the investigation of ferroaxial order and three-dimensionally visualizing its domain states.

METHODS

Sample preparation

Single crystals of NiTiO_3 were grown by the flux method. Details of the growth procedures are described in ref. ¹². The obtained crystals were plate-shaped with typical dimensions of $3 \times 3 \times 0.1 \text{ mm}^3$

and were confirmed to be ilmenite-type NiTiO_3 by X-ray diffraction measurements. The widest faces of the crystals were perpendicular to the c -axis (hexagonal setting). The as-grown crystals are usually composed of a single ferroaxial domain state. To form multi-domain states, the as-grown crystals were annealed in air from 1623 K at a cooling rate of 1 K h^{-1} . The annealed crystals were polished down to the thickness of 20–60 μm for SHG measurements.

Second harmonic generation microscopy

CID-SHG measurements were performed at room temperature by a scanning transmission microscope. The fundamental light was provided by a femtosecond optical parametric oscillator TOPOL (Avesta) which can produce wavelengths of 680–1000 nm and 1100–2300 nm. In the present study, we mainly used a wavelength of 1200 nm with a repetition frequency of 80 MHz and a pulse width of 125 fs. The power of fundamental light was adjusted by an attenuator, which was composed of a combination of a half-wave plate and a Gran-Taylor prism. The circularly polarized light was produced by a quarter-wave plate and its degree of circular polarization was confirmed to be about 90 %. A pair of objectives with a numerical aperture of 0.65 and a pinhole were used to make a confocal system. The SH intensity was collected by a point detector using a photon counting method. Two-dimensional images of the SH intensity were obtained by scanning an incident wave using a galvanometer scanner. A scanning motor was used to collect two-dimensional images with different depths and constructed three-dimensional images. The spatial resolutions of our system are around 0.56 μm for lateral direction and 3 μm for depth direction.

DATA AVAILABILITY

The data that support the findings of this study are available from the corresponding author upon reasonable request.

Received: 5 August 2022; Accepted: 14 October 2022;

Published online: 03 November 2022

REFERENCES

- Aizu, K. Possible species of ferromagnetic, ferroelectric, and ferroelastic crystals. *Phys. Rev. B* **2**, 754–772 (1970).
- Schmid, H. Some symmetry aspects of ferroics and single phase multiferroics. *J. Phys.: Condens. Matter* **20**, 434201 (2008).
- Johnson, R. D. et al. $\text{Cu}_3\text{Nb}_2\text{O}_6$: A multiferroic with chiral coupling to the crystal structure. *Phys. Rev. Lett.* **107**, 137205 (2011).
- Hlinka, J., Privratska, J., Ondrejčovič, P. & Janovec, V. Symmetry guide to ferroaxial transitions. *Phys. Rev. Lett.* **116**, 177602 (2016).
- Cheong, S.-W., Talbayev, D., Kiryukhin, V. & Saxena, A. Broken symmetries, non-reciprocity, and multiferroicity. *npj Quantum Mater.* **3**, 19 (2018).
- Dubovik, V. M. & Tugushkov, V. V. Toroid moments in electrodynamics and solid-state physics. *Phys. Rep.* **187**, 145–202 (1990).
- Naumov, I. I., Bellaiche, L. & Fu, H. Unusual phase transitions in ferroelectric nanodisks and nanorods. *Nature* **432**, 737–740 (2004).
- Prosandeev, S., Ponomareva, I., Kornev, I., Naumov, I. & Bellaiche, L. Controlling toroidal moment by means of an inhomogeneous static field: An ab initio study. *Phys. Rev. Lett.* **96**, 237601 (2006).
- Jin, W. et al. Observation of a ferro-rotational order coupled with second-order nonlinear optical fields. *Nat. Phys.* **16**, 42–46 (2020).
- Luo, X. et al. Ultrafast modulations and detection of a ferro-rotational charge density wave using time-resolved electric quadrupole second harmonic generation. *Phys. Rev. Lett.* **127**, 126401 (2021).
- Hayashida, T. et al. Visualization of ferroaxial domains in an order-disorder type ferroaxial crystal. *Nat. Commun.* **11**, 4582 (2020).
- Hayashida, T. et al. Phase transition and domain formation in ferroaxial crystals. *Phys. Rev. Mater.* **5**, 124409 (2021).
- Cheong, S.-W., Lim, S., Du, K. & Huang, F.-T. Permutable SOS (symmetry operational similarity). *npj Quantum Mater.* **6**, 58 (2021).

- Hayami, S., Oiwa, R. & Kusunose, H. Electric ferro-axial moment as nanometric rotator and source of longitudinal spin current. *J. Phys. Soc. Jpn.* **91**, 113702 (2022).
- Nasu, J. & Hayami, S. Antisymmetric thermopolarization by electric toroidicity. *Phys. Rev. B* **105**, 245125 (2022).
- Shen, Y. R. *Principles of Nonlinear Optics* (Wiley, New York, 1984).
- Fiebig, M., Pavlov, V. V. & Pisarev, R. V. Second-harmonic generation as a tool for studying electronic and magnetic structures of crystals: Review. *J. Opt. Soc. Am. B* **22**, 96–118 (2005).
- Araoka, F. et al. Twist-grain-boundary structure in the B_4 phase of a bent-core molecular system identified by second harmonic generation circular dichroism measurement. *Phys. Rev. Lett.* **94**, 137801 (2005).
- Lee, H. et al. Chiral imaging of collagen by second-harmonic generation circular dichroism. *Biomed. Opt. Exp.* **4**, 909–916 (2013).
- Schmeltz, M. et al. Circular dichroism second-harmonic generation microscopy probes the polarity distribution of collagen fibrils. *Optica* **7**, 1469–1476 (2020).
- Fiebig, M. et al. Second harmonic generation in the centrosymmetric antiferromagnet NiO . *Phys. Rev. Lett.* **87**, 137202 (2001).
- Cherian, J. G., Tokumoto, T. D., Zhou, H., Choi, E. S. & McGill, S. A. Electronic structure and magnetic symmetry in MnTiO_3 analyzed by second harmonic generation. *Phys. Rev. B* **87**, 214411 (2013).
- Boysen, H., Frey, F., Lerch, M. & Vogt, T. A neutron powder investigation of high-temperature phase transition in NiTiO_3 . *Z. Fur Krist.* **210**, 328–337 (1995).
- Birss, R. R. *Symmetry and Magnetism* (North-Holland, Amsterdam, 1964).
- Yokota, H. & Uesu, Y. Optical second-harmonic generation microscopy as a tool for ferroelastic domain wall exploration. *J. Appl. Phys.* **129**, 014101 (2021).
- Low, W. Paramagnetic and optical spectra of divalent nickel in cubic crystalline fields. *Phys. Rev.* **109**, 247–255 (1985).
- Rossmann, G. R., Shannon, R. D. & Waromg, R. K. Origin of the yellow color of complex nickel oxides. *J. Solid State Chem.* **39**, 277–287 (1981).
- Van Aert, S. et al. Direct observation of ferrielectricity at ferroelastic domain boundaries in CaTiO_3 by electron microscopy. *Adv. Mater.* **24**, 523–527 (2012).
- Yokota, H. et al. Direct evidence of polar nature of ferroelastic twin boundaries in CaTiO_3 obtained by second harmonic generation microscope. *Phys. Rev. B* **89**, 144109 (2014).
- Yokota, H., Matsumoto, S., Salje, E. K. H. & Uesu, Y. Symmetry and three-dimensional anisotropy of polar domain boundaries observed in ferroelastic LaAlO_3 in the complete absence of ferroelectric instability. *Phys. Rev. B* **98**, 104105 (2018).
- Sheng, Y. et al. Three-dimensional ferroelectric domain visualization by Čerenkov-type second harmonic generation. *Opt. Express* **18**, 16539–16545 (2010).
- Kämpfe, T. et al. Optical three-dimensional profiling of charged domain walls in ferroelectrics by Čerenkov second-harmonic generation. *Phys. Rev. B* **89**, 035314 (2014).
- Momma, K. & Izumi, F. VESTA 3 for three-dimensional visualization of crystal, volumetric, and morphology data. *J. Appl. Crystallogr.* **44**, 1272–1276 (2011).

ACKNOWLEDGEMENTS

We thank Y. Uesu, D. Morikawa, and K. Tsuda for helpful discussions. The schematic illustrations of crystal structures were drawn by using the software VESTA³³. This work was supported by JSPS KAKENHI Grants JP19H05823, JP21H04436, JP21H01010, and JP22J11247. This work was partially supported by JST PRESTO Grants Number JPMJPR19LA, Japan.

AUTHOR CONTRIBUTIONS

H.Y., T.H., and T.K. designed research. T.H. performed crystal growth, sample preparation, and electrogyration measurements. H.Y. and D.K. carried out measurements of optical second harmonic generation. H.Y. and T.K. prepared the manuscript, and all authors discussed and contributed to the final manuscript.

COMPETING INTERESTS

The authors declare no competing interests.

ADDITIONAL INFORMATION

Supplementary information The online version contains supplementary material available at <https://doi.org/10.1038/s41535-022-00515-w>.

Correspondence and requests for materials should be addressed to Hiroko Yokota.

Reprints and permission information is available at <http://www.nature.com/reprints>

Publisher's note Springer Nature remains neutral with regard to jurisdictional claims in published maps and institutional affiliations.



Open Access This article is licensed under a Creative Commons Attribution 4.0 International License, which permits use, sharing, adaptation, distribution and reproduction in any medium or format, as long as you give appropriate credit to the original author(s) and the source, provide a link to the Creative Commons license, and indicate if changes were made. The images or other third party material in this article are included in the article's Creative Commons license, unless indicated otherwise in a credit line to the material. If material is not included in the article's Creative Commons license and your intended use is not permitted by statutory regulation or exceeds the permitted use, you will need to obtain permission directly from the copyright holder. To view a copy of this license, visit <http://creativecommons.org/licenses/by/4.0/>.

© The Author(s) 2022